



Ligand-based design and synthesis of novel sodium channel blockers from a combined phenytoin–lidocaine pharmacophore

Yuesheng Wang^a, Paulianda J. Jones^a, Timothy W. Batts^b, Victoria Landry^a, Manoj K. Patel^b, Milton L. Brown^{c,d,e,*}

^a Department of Chemistry, University of Virginia, Charlottesville, VA 22904, USA

^b Department of Anesthesiology, University of Virginia, Charlottesville, VA 22904, USA

^c Department of Oncology, Georgetown University Medical Center, 3970 Reservoir Road, Washington, DC 20057, USA

^d Department of Neuroscience, Georgetown University Medical Center, 3970 Reservoir Road, Washington, DC 20057, USA

^e Drug Discovery Program, 3970 Reservoir Road, Washington, DC 20057, USA

ARTICLE INFO

Article history:

Received 22 April 2008

Revised 3 October 2008

Accepted 3 October 2008

Available online 17 October 2008

Keywords:

Sodium channels

CoMFA

Antagonist

Electrophysiology

ABSTRACT

The voltage-gated sodium channel remains a rich area for the development of novel blockers. In this study we used comparative molecular field analysis (CoMFA), a ligand-based design strategy, to generate a 3D model based upon local anesthetics, hydantoins, and α -hydroxyphenylamides to elucidate a SAR for their binding site in the neuronal sodium channel. Correlation by partial least squares (PLS) analysis of in vitro sodium channel binding activity (expressed as pIC_{50}) and the CoMFA descriptor column generated a final non-cross-validated model with $q^2 = 0.926$ for the training set. The CoMFA steric and electrostatic maps described a binding site predominately hydrophobic in nature. This model was then used to design and predict a series of novel sodium channel blockers that utilized overlapping structural features of phenytoin, hydroxy amides, and the local anesthetic lidocaine. Synthesis and evaluation of these compounds for their ability to inhibit [³H]-batrachotoxin revealed that these compounds have potent sodium channel blockade. Furthermore, the CoMFA model was able to accurately predict the binding of these compounds to the neuronal sodium channel. Synthesis and subsequent sodium channel evaluation of compound 37 (predicted $IC_{50} = 7 \mu M$, actual $IC_{50} = 6 \mu M$), established that novel compounds based on overlapping regions of phenytoin and lidocaine are better binders to the sodium channel than phenytoin itself ($IC_{50} = 40 \mu M$).

© 2009 Published by Elsevier Ltd.

1. Introduction

Neuronal voltage-gated sodium channels (NVSC) play an important role in the generation and propagation of action potentials in neurons and other excitable cells. Thus, NVSC blocking agents represent a clinically important class of drugs used in the treatment of pain, seizures and arrhythmia.

Cloning, purification and sequence analysis of NVSCs have identified at least ten highly conserved α -subunits. The NVSC is composed of six transmembrane segments (S1–S6) that form the 260 kDa α -subunit complex and at least four important accessory β -subunits.¹

Information concerning channel topography has been obtained through the use of neurotoxins. In fact, voltage-sensitivity is characterized based on the channel's sensitivity to tetrodotoxin (TTX), a

* Corresponding author. Address: Departments of Oncology and Neuroscience, Georgetown University Medical Center, 3970 Reservoir Road, Washington, DC 20057, USA. Tel.: +1 202 687 8603.

E-mail address: mb544@georgetown.edu (M.L. Brown).

deadly neurotoxin of the puffer fish. The binding site for batrachotoxin (BTX), an alkaloid from poison dart frogs, binds to the inactivated state of the NVSC, thereby disrupting the equilibrium of protein states. Substitution with a para-[³H] benzoate ester at C₂₀ on BTX resulted in the development of a very useful radioligand [³H]-BTX-B.² The binding of [³H]-BTX-B to the NVSC protein is allosterically linked³ to and overlaps with the binding sites of both anticonvulsants (phenytoin) and local anesthetics (lidocaine). Functionally, BTX stabilizes the NVSCs in their open conformation, whereas local anesthetics block Na⁺ conductance.

The use of [³H]-BTX-B as a NVSC screening tool has indicated an important relationship between molecular structure and pharmacological effects for interactions of small molecule inhibitors. Using this information, a ligand-based molecular modeling study was successful in the design of a new small molecule which binds potently ($IC_{50} = 9 \mu M$) to the NVSC^{4–6} and a relationship between [³H]-BTX-B inhibition and anticonvulsant activity in mice has been established.⁷

Site-directed mutagenesis studies have identified clusters of common residues at D1–S6, D3–S6, and D4–S6 segments within

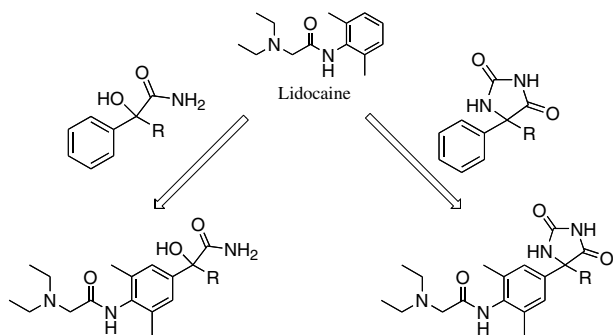


Figure 1. Design of novel grafted phenytoin/lidocaine compounds.

the NVSC α -subunit that are critical for binding of hydantoin (phenytoin) and local anesthetics (lidocaine).^{8,9} Mutations of amino acid residues in specific segments of the α -subunit have revealed important voltage dependence and modification of protein conformational states (open, inactivated, closed).¹⁰ Altogether, these studies suggest that phenytoin and lidocaine share a non-identical but overlapping receptor¹¹ on the extracellular side of the NVSC.¹²

Considering the accepted overlapping nature of the binding sites of phenytoin and lidocaine, we have employed the use of comparative molecular field analysis (CoMFA) to assist in identifying important overlapping structural features and to provide insight into essential SAR for the development of novel NVSC inhibitors. CoMFA, a 3D ligand-based discovery program is useful in correlating biological activity with structural features and has become a valuable tool in the design of new inhibitors of biological receptors. In this study, we have pro-

posed a series of novel grafted phenytoin/lidocaine and hydroxyamide/lidocaine compounds (Fig. 1) that were identified and predicted by CoMFA to have potent NVSC activity. We have validated our CoMFA alignment by synthesizing these proposed compounds and evaluating them for inhibition of [³H]-BTX-B.

2. Results

Our previous sodium channel SAR studies suggested that $\log P$ was one of the parameters important for enhanced binding to the NVSC.⁵ In the training set, $\log P$ correlation to pIC_{50} gave an R^2 of 0.59 (Fig. 3). This is poor correlation, in fact, the groups of compounds at $\log P \approx 2.5$ and $\log P \approx 3.0$ have IC_{50} values that span 2 log units. It is clear that local anesthetic binding to the NVSC is dependent on other factors besides lipophilicity. Comparisons within the present model of local anesthetics and hydantoin with the same $\log P$ and different structures often show very different binding affinities to the NVSC (e.g. **3** and piperocaine). We were thus encouraged to use CoMFA to investigate the differences in structural and electrostatic features of these analogues in an effort to formulate an improved model. The sodium channel binding affinities and lipophilicities for the CoMFA training set are presented in Table 1. PLS correlation of in vitro sodium channel binding, expressed as $-\log IC_{50}$, and CoMFA descriptors generated a CoMFA model with $q^2 = 0.926$ for the training set (Fig. 4). Further more, the CoMFA model provided better correlation than that for the $\log P$ model ($R^2 = 0.59$) from the same data set.

Investigations of the CoMFA steric map revealed that a long alkyl chain at the C5 position appears to be required for tight binding to the hydantoin site. The steric contour map in Figure 5 reveals a

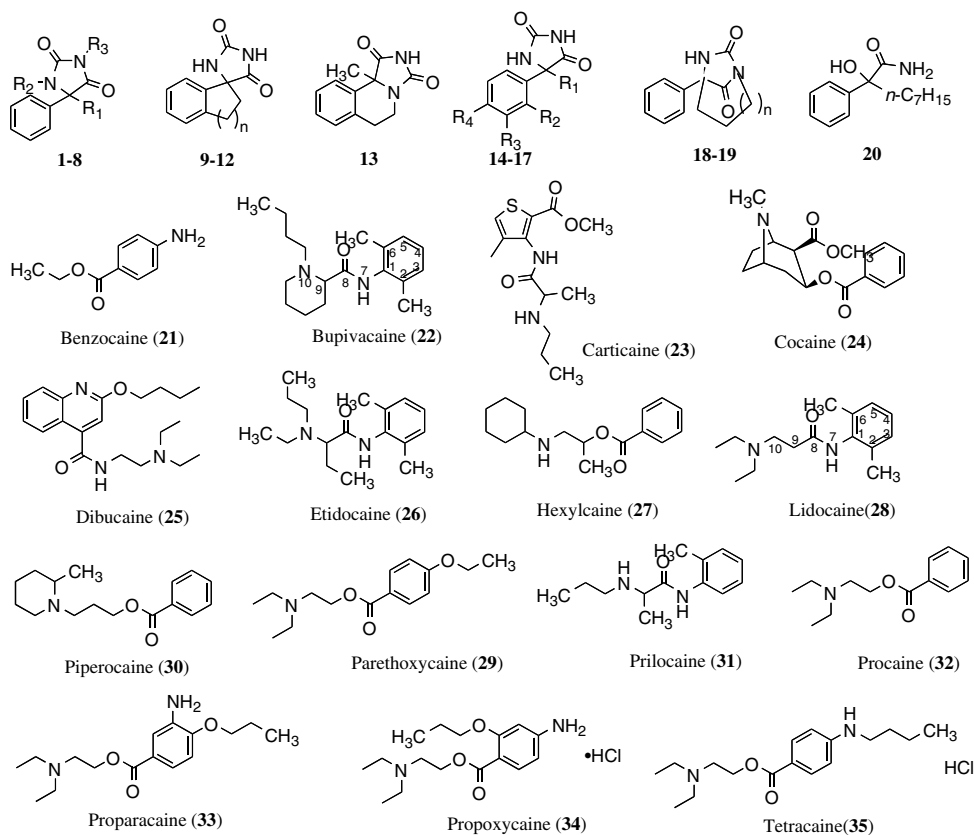


Figure 2. Test set compounds used in developing the CoMFA model.

Table 1
Sodium channel binding activities for the training set used in the final non-cross-validated CoMFA model^a

Compound	R ₁	R ₂	R ₃	R ₄	n	LogP	³ H-BTX IC ₅₀ (μM)	Final model, -pIC ₅₀ ^b		
								Obsd	Pred	Res
1	<i>n</i> -Propyl	H	H			1.96	162	-2.21	-2.10	-0.11
2	<i>n</i> -Butyl	H	H			2.46	103	-2.01	-1.91	-0.10
3	<i>n</i> -Butyl	H	H			3.01	285	-2.45	-2.16	-0.30
4	<i>n</i> -Pentyl	H	Methyl			2.96	39	-1.59	-1.55	-0.04
5	<i>n</i> -Hexyl	H	H			3.40	13	-1.11	-1.17	0.06
6	<i>n</i> -Heptyl	H	H			3.96	5	-0.70	-0.82	0.12
7	<i>n</i> -Nonyl	H	H			4.96	5	-0.70	-0.54	-0.16
8	Methyl	Ethyl	H			2.02	720	-2.86	-2.87	0.01
9					1	0.96	2112	-3.32	-2.87	-0.46
10					2	1.46	851	-2.93	-2.66	-0.27
11					3	1.96	251	-2.40	-2.52	0.12
12					4	2.46	251	-2.40	-2.43	0.03
13						1.52	250	-2.40	-2.46	0.06
14	<i>n</i> -Butyl	Methyl	H	H		2.96	225	-2.35	-2.03	-0.33
15	<i>n</i> -Butyl	H	Methyl	H		2.96	58	-1.76	-1.78	0.02
16	<i>n</i> -Butyl	H	H	Methyl		2.96	95	-1.98	-2.22	0.25
17	Cyclohexyl	H	H	H		2.96	58	-1.76	-1.91	0.14
18					2	2.01	700	-2.85	-3.11	0.27
19					3	2.51	427	-2.63	-2.79	0.16
20						3.70	9	-0.95	-0.96	0.01
21						1.39	910	-2.96	-3.10	0.14
22						3.86	5.4	-0.73	-0.95	0.22
23							51	-1.71	-1.65	-0.06
24						1.82	49	-1.69	-1.71	0.02
25						3.77	1.4	-0.15	0.22	-0.37
26						3.87	3.5	-0.54	-0.99	0.44
27						3.34	7.1	-0.85	-0.81	-0.04
28						2.70	240	-2.38	-1.94	-0.44
29						2.74	24	-1.38	-1.12	-0.26
30						3.01	12.9	-1.11	-0.86	-0.25
31						2.18	53.7	-1.73	-1.81	0.08
32						2.53	109.6	-2.04	-1.96	-0.08
33						2.42	2	-0.28	-0.72	0.44
34						2.42	24	-1.38	-1.50	0.12
35						3.27	3.4	-0.53	-0.73	0.20
36						2.46	40	-1.60	-1.95	0.35

^a Number of components = 4; *s* = 0.245; *q*² = 0.926.

^b -pIC₅₀ = -log IC₅₀.

favorable steric volume near the 5-alkyl side chain. In addition, steric bulk in the amide portion of the local anesthetics appears to also be favorable as revealed by comparison of binding by benzocaine (IC₅₀ = 910 μM) and etidocaine (IC₅₀ = 3.5 μM) to the local anesthetic site.

An important part of a 3D-QSAR model is the ability to accurately predict the relative binding potencies of novel analogues before synthesis. Based upon the model described here, we proposed that novel analogues containing both the

phenytoin (hydantoin) pharmacophore or the hydroxyamide pharmacophore and the local anesthetic lidocaine would be potent binders to the neuronal sodium channel as they would potentially have the ability to bind to an expanded binding region encompassing both the phenytoin and local anesthetic binding sites. Using the CoMFA model described above, our newly developed grafted analogues were predicted to have IC₅₀ values of 3 μM (**40**) to 66 μM (**38**) (Table 3).

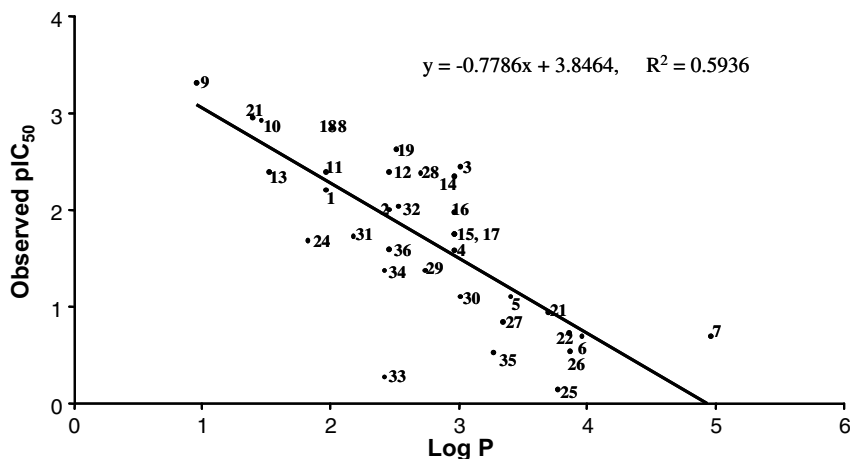


Figure 3. Plot of logP versus pIC₅₀ for compounds in the training set.

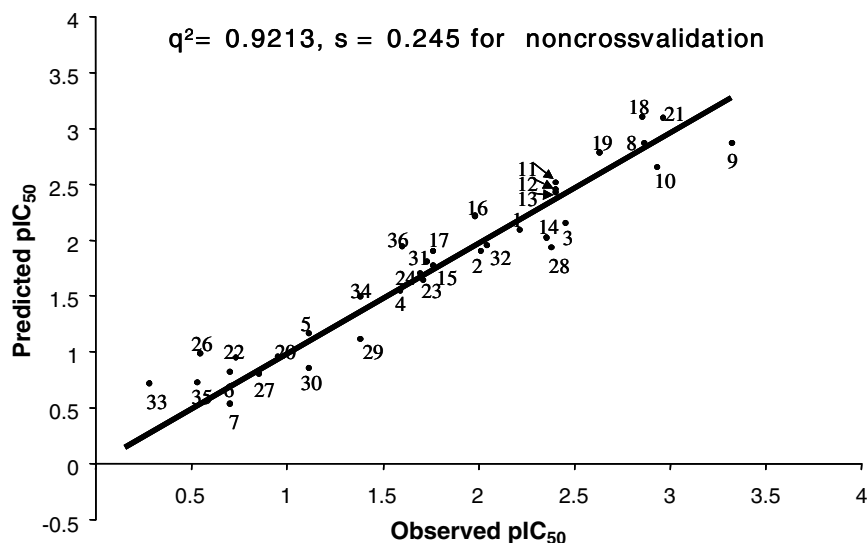


Figure 4. Plot of observed pIC_{50} versus predicted pIC_{50} values for the non-cross-validated CoMFA model in Table 1.

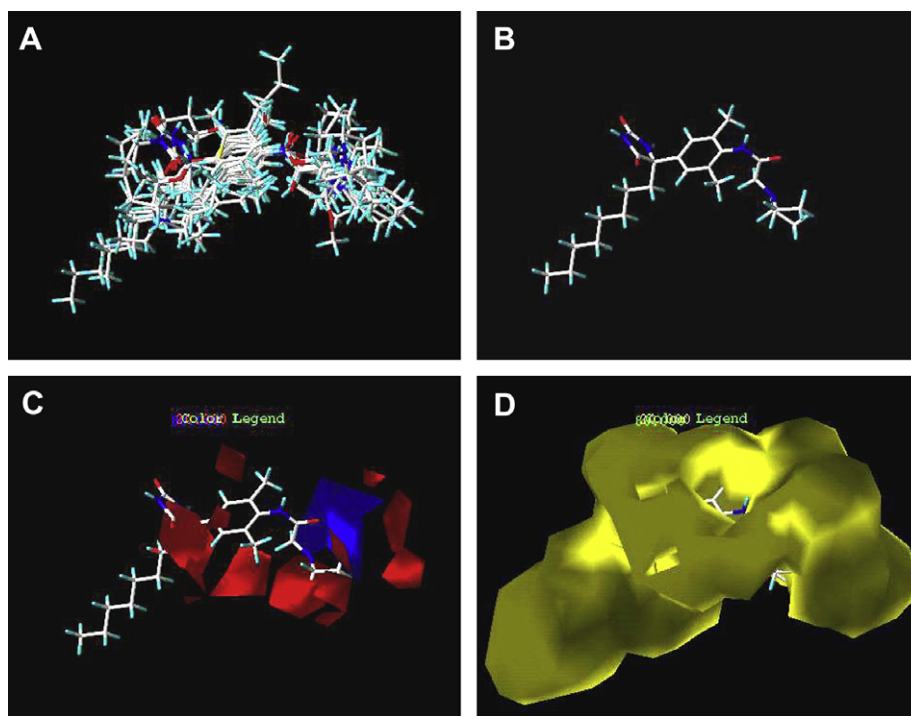
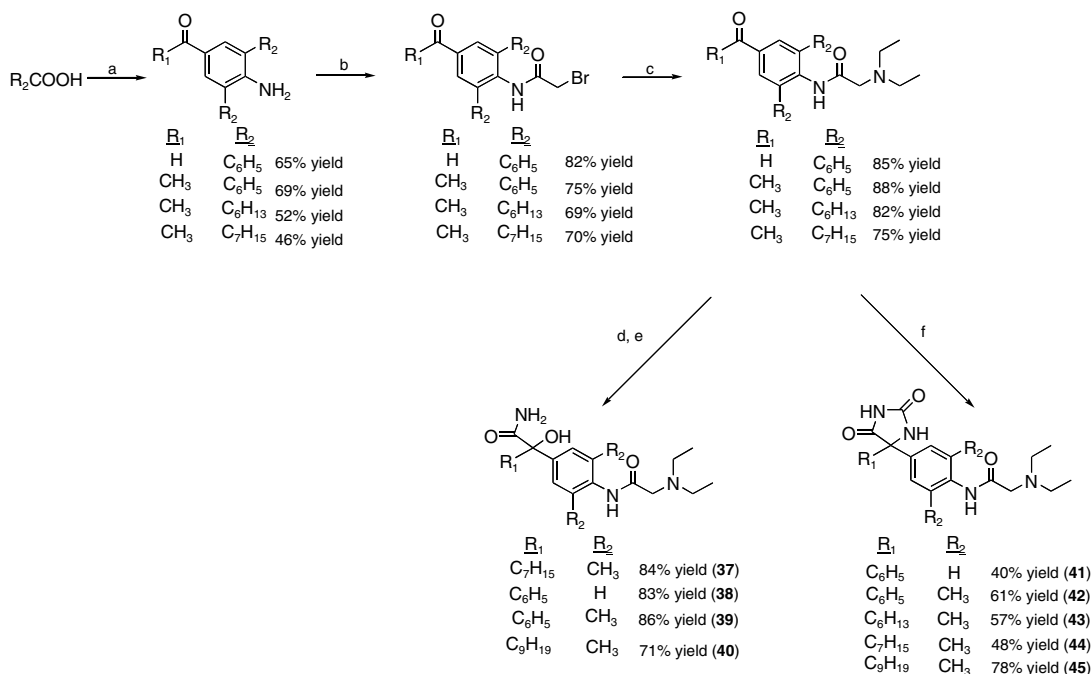


Figure 5. Electrostatic and steric CoMFA fields for the model developed from compounds in Table 1. For electrostatic contours, increased binding results from placing more positive (+) charge near blue and negative (–) charge near red. For steric contours increased binding results from placing more bulk near green and less bulk near yellow. (A) Overlay of compounds used in the training set. (B) Active analogue **44**. (C) Active analogue **44** with electronic contour overlay. (D) Active analogue **44** with steric contour overlay.

After successfully completing the syntheses of analogues **37–45** (Scheme 1) we evaluated them for activity using [3H]-BTX-B binding assay with each compound at a concentration of $40\ \mu M$ (IC_{50} of phenytoin in this assay). This series of analogues encompasses a range of lipophilicities ($\log P = 1.4–5.3$) as well as phenyl ring substitutions ($R_2 = H$ or CH_3), pharmacophore changes (hydroxyamides vs hydantoin), and chain length ($R_1 = Ph, C_6H_{13}, C_7H_{15},$ and C_9H_{19}). The predictive ability of the CoMFA model was evaluated by comparing the observed versus predicted activities of the novel hybrid phenytoin/lidocaine and hydroxyamide/lidocaine analogues.

Observed [3H]-BTX displacement revealed that compound **37** displaced 83% [3H]-BTX at $40\ \mu M$. Compounds **41** and **42**, the direct grafts of phenytoin and lidocaine, displaced 50 and 49% [3H]-BTX, respectively. As a comparison between the hydroxyamides and hydantoin, compound **44** (hydantoin analogue of **37**) displaced 71% [3H]-BTX at $40\ \mu M$. The latter data is shown in Table 3, and these four analogues were chosen based on their potent inhibition at $40\ \mu M$ and to allow comparisons between direct phenytoin/lidocaine grafts and hydroxyamide/hydantoin pharmacophores. As previously mentioned, compounds **37** and **44** represent optimal binders based upon initial [3H]-BTX data when tested at a concen-



Scheme 1. Reagents and conditions: (a) PPA, 180–200 °C; (b) bromoacetyl bromide, DMAP, THF; (c) diethylamine, NaHCO₃, KI, MeOH; (d) (1) TMSCN, KCN, 18-Crown-6, (2) 15% HCl; (e) 1,4-dioxane, HCl, HCl (g); (f) KCN, (NH₄)₂CO₃, EtOH, 60–65 °C.

tration of 40 μM (IC₅₀ of phenytoin). Compounds **41** and **42** represent grafts of phenytoin and lidocaine with and without the phenyl ring methyl groups of lidocaine. It is evident from this data that the CoMFA model has excellent predictive ability. Residual values (the difference between the observed IC₅₀ and the predicted IC₅₀) ranged from 0.05 to 0.26 for these novel compounds. As expected, compounds **37** and **44**, which were designed to take advantage of the steric requirement at C5 with a long alkyl chain demonstrating the best activity with IC₅₀ values of 6.0 and 13.5 μM, respectively. Compounds **41** and **42** showed identical IC₅₀ values of about 39.8 μM (predicted = 44.7 and 50.1 μM, respectively). It should be noted that when tested at 40 μM in the preliminary [³H]-BTX assay, these two compounds showed [³H]-BTX displacement of 50% and 49%, further validating the predictive ability of the CoMFA model. Compound **42** was designed as a direct graft of the anticonvulsant phenytoin and the local anesthetic lidocaine. The sodium channel binding potency of this analogue was correctly predicted by the CoMFA model (observed IC₅₀ = 39.8 μM). Interestingly, the IC₅₀ of lidocaine in this assay is 240 μM and that of phenytoin is 40 μM, thus this analogue increases the binding potency of the lidocaine moiety 6-fold.

In comparing the inhibition of BTX binding to Na⁺ channels between the hydroxyamides (**37–40**) and hydantoin (**41–45**), it is apparent that when R₁ is a phenyl group, hydantoin are much more active than the corresponding hydroxyamides. This difference cannot be solely attributed to lipophilicity as the log*P* values for these lidocaine analogues are all within one log unit of one another (1.4–2.5).

Substitution of a heptyl group for the phenyl group at R₁ in the lidocaine/hydroxyamide analogues (**37** vs **39**) resulted in a greater than 5-fold increase in inhibition (83% vs 16%). Similarly, the lidocaine/hydantoin analogue showed an increase in inhibition (49% for R₁ = Ph vs 71% for R₁ = heptyl) but it was not nearly as dramatic as that seen in the other analogues. The substitution of a heptyl group for a phenyl group corresponds to both an increase in size as well as lipophilicity (~1.5-fold increase in log*P*). The heptyl substitution appears to remain the optimal substituent

in this region, as increasing the chain length to 9 carbons (**37** vs **40**) actually results in a less potent compound. Interestingly, in the lidocaine/hydantoin analogue, the series of 6, 7, to 9 carbon chains at R₁ showed no difference in potency. This result appears to support our previous findings that hydantoin within the same class having similar log*P* values exhibit similar binding potencies.⁷

We determined the effects of compound **37** on sodium currents recorded from HEK cells stably expressing human Na_v1.2. At a concentration of 100 μM compound **37** exhibited a 67.7% ± 5.6% (*n* = 4) block of sodium channel current (Fig. 6) and were fully reversible on washout. These results demonstrate that the newly designed compound **37** has significant functional effects on inhibiting sodium channel currents.

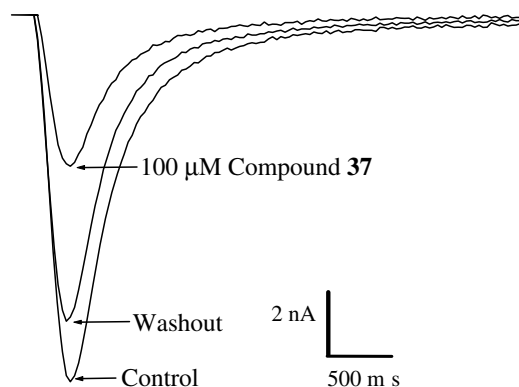


Figure 6. Sample current traces shows block by compound **37** of the human Na_v1.2 sodium channel isoform stably expressed in HEK 293 cells. Currents were elicited by a step depolarization to +10 mV for 12 ms from a holding potential of −100 mV. Compound **37** blocked 67.7 ± 5.6% (*n* = 4) of the recorded current which was partially reversible upon washout.

3. Discussion

Voltage-gated sodium channels are important in many physiological processes and their dysregulation are known to play a key role in several pathological human diseases.¹³ In view of this, voltage-gated sodium channels remain an attractive target for medicinal chemistry. Since the X-ray structure of the voltage-gated sodium channel remains unsolved, the development of computer based strategies that contribute to the design of new sodium channel ligands are critical in our pursuit of targeted inhibitors. The CoMFA analysis presented in this study provides such a model and allowed us to encompass a range of new structures. The predictive sodium channel binding affinities for four novel compounds not present in the training set and not previously reported provided a focused rationale for targeted synthesis. The novel synthetic compounds were evaluated for direct displacement of a sodium channel specific radioligand and function block of cellular sodium channel currents was confirmed for one lead. Both the ³H-BTX and the electrophysiology confirms our hypothesis for targeting site 2 of the sodium channel and our study provides validation of this technique with functional sodium channel block. Finally, this study expands our understanding concerning the binding region encompassing both the local anesthetic and anticonvulsant binding sites within site 2 of the sodium channel.

4. Conclusion

One of the most challenging facets of ion channel drug discovery is the design of new classes of small molecule leads with appropriate potency without the direct assistance of 3D protein X-ray structures. In this study we have used ligand-based drug design through CoMFA and validated the model by synthesis and evaluation of human sodium channel interactions. This finding continues to support the use of CoMFA in transmembrane drug discovery paradigms where little or no target structural data is known.

5. Experimental

All reaction requiring anhydrous conditions were carried out in flame-dried glassware under nitrogen atmosphere. Solvents were purified by pressure filtration through activated alumina. Melting points were determined in open capillary tubes with an electrothermal Mel-temp melting point apparatus and are uncorrected. ¹H and ¹³C NMR spectra were measured on a General Electric 300 MHz spectrometer. Chemical shifts are reported in ppm relative to resonances of the solvent CDCl₃ (unless specified otherwise): 7.25 ppm in the ¹H spectra and 77.08 ppm in the ¹³C spectra.

Thin-layer chromatography was performed on silica gel 60 F 254 aluminum sheets with UV detection. Chromatography separations were carried out on silica gel columns (silica gel 60, 40–63 μm).

Mass spectra were obtained on Thermofinnigan LCQ iontrap (Classic) instrument. High-resolution mass spectrometry was performed at the University of Illinois at Urbana-Champaign, School of Chemical Science.

5.1. General procedure for the preparation of 4-aminobenzophenones

A mixture of 2,6-dimethylaniline (1.0 equiv), RCOOH (2.0 equiv) in excess PPA was heated with vigorous stirring at 180–200 °C for 1 h. Then, 2N hydrochloric acid and water was added and stirred for an additional hour. The reaction was cooled to 25 °C and extracted with CH₂Cl₂, dried over MgSO₄, filtered, and concentrated. The residue was purified by silica gel column chromatography, eluting with EtOAc/hexane.

5.2. General procedure for the preparation of lidocaine-ketones

To a solution of bromoacetyl bromide (1.5 equiv) in THF at 0 °C was added dropwise, under stirring and nitrogen atmosphere, a solution of R-NH₂ (1.0 equiv) and 4-(dimethylamino)pyridine (0.5 equiv) in THF. The reaction mixture was stirred at 0 °C for 1.5 h, then at room temperature for 1 h. The reaction was quenched with water and extracted with CH₂Cl₂, dried over MgSO₄, filtered, and concentrated by rotary evaporator. The crude product was purified by silica gel column chromatography, eluting with EtOAc/hexane.

A solution of above product (1.0 equiv), diethylamine (1.5 equiv), sodium bicarbonate (1.5 equiv), and potassium iodide (catalytic amount) in methanol was stirred at 50 °C for 4 h. The reaction mixture was cooled to room temperature and diluted with ethyl acetate and water, then the mixture was extracted with CH₂Cl₂, dried over MgSO₄, filtered, and concentrated. The residue was purified by silica gel column chromatography, eluting with EtOAc/hexane.

5.3. General procedure for the preparation of α-hydroxyamides (37–40)

To a solution of the ketone (1.0 equiv) in CH₂Cl₂ were added KCN and 18-Crown-6 (10 mg per mol of ketone) and trimethylsilylcyanide (2.5 equiv) by syringe under nitrogen atmosphere. The reaction mixture was stirred for 24 h at 25 °C. After 24 h. the solvent was removed in vacuo.

To the residue was added 1,4-dioxane (5 ml per mmol of ketone) and cooled to 0 °C. Previously cooled concentrated HCl (1 ml per 1 mmol of ketone) was added and HCl gas (from H₂SO₄ and NH₄Cl) was then passed through the reaction mixture for 1 h at 0 °C. The mixture was allowed to stand at room temperature overnight then extracted with CH₂Cl₂. The extracts were dried over MgSO₄, filtered, concentrated, and purified by silica gel column chromatography, eluting with EtOAc/hexane.

5.3.1. 2-[4-(2-Diethylamino-acetyl-amino)-3,5-dimethyl-phenyl]-2-hydroxy-nonanoic acid amide (37)

Isolated as a light brown oil. ¹H NMR: δ 9.20–8.39 (s, 1H), 7.78–7.23 (s, 1H), 7.04–6.94 (s, 1H), 6.74–6.64 (s, 1H), 6.30–6.20 (s, 1H), 2.65–2.48 (s, 2H), 2.49–2.33 (m, 4H), 1.65–1.49 (m, 2H), 1.91–1.75 (s, 6H), 1.02–0.84 (m, 14H), 0.84–0.71 (t, *J* = 7.5 Hz, 6H), 0.58–0.46 (t, *J* = 6 Hz, 3H); ¹³C NMR: δ 177.97, 162.83, 142.56, 134.60, 133.18, 125.66, 78.42, 49.14, 36.59, 32.07, 31.45, 30.08, 29.44, 22.84, 18.93, 14.32, 12.30; HRMS (EI): calcd for C₂₃H₃₉N₃O₃ 405.5809; found, 405.5811.

5.3.2. 2-[4-(2-Diethylamino-acetyl-amino)-phenyl]-2-hydroxy-2-phenyl-acetamide (38)

Isolated as a light brown oil (40%). ¹H NMR: δ 9.69–8.91 (s, 1H), 7.52–6.47 (m, 9H), 3.03–2.82 (s, 2H), 2.62–2.41 (m, 4H), 1.06–0.86 (t, *J* = 6 Hz, 6H); ¹³C NMR: δ 176.93, 170.96, 143.78, 139.45, 137.43, 128.87, 128.43, 128.13, 119.34, 70.52, 58.32, 49.31, 12.86; HRMS (EI): calcd for C₂₀H₂₅N₃O₃ 355.4358; found 355.4357.

5.3.3. 2-[4-(2-Diethylamino-acetyl-amino)-3,5-dimethyl-phenyl]-2-hydroxy-2-phenylacetamide (39)

Isolated as a light brown oil (61%). ¹H NMR: δ 9.42–8.20 (s, 1H), 7.53–7.39 (m, 2H), 7.39–7.34 (m, 3H), 7.20–7.07 (s, 2H), 6.63–6.35 (s, 1H), 6.08–5.80 (s, 1H), 3.29–2.97 (s, 2H), 2.80–2.54 (m, 4H), 2.23–2.06 (s, 6H), 1.25–1.00 (t, *J* = 6 Hz, 6H); ¹³C NMR: δ 176.8, 171.18, 143.15, 142.14, 135.45, 134.19, 128.61, 128.36, 128.03, 127.99, 81.47, 57.79, 49.44, 19.22, 13.11; HRMS (EI): calcd for C₂₂H₂₉N₃O₃ 383.4906; found 383.4905.

5.3.4. 2-[4-(2-Diethylamono-acetylamono)-3,5-dimethyl-phenyl]-2-hydroxy-undecanoic acid amide (40)

Isolated as a light yellow oil (71%). ¹H NMR: δ 9.21–8.41 (s, 1H), 7.55–6.92 (s, 2H), 6.99–6.41 (s, 1H), 6.32–5.89 (s, 1H), 3.56–3.30 (s, 2H), 3.16–2.90 (t, J = 9 Hz, 2H), 2.68–2.42 (m, 4H), 2.19–1.99 (s, 6H), 1.35–1.10 (m, 14H), 1.09–1.049 (t, J = 6 Hz, 6H), 0.89–0.63 (t, J = 6 Hz, 3H); ¹³C NMR: δ 178.01, 170.93, 142.48, 134.92, 133.42, 125.94, 78.61, 57.83, 49.38, 39.58, 32.31, 32.20, 30.36, 30.07, 29.97, 29.74, 23.07, 19.16, 14.52, 13.04. HRMS (EI): calcd for C₂₅H₄₃N₃O₃ 433.6352; found, 433.6353.

5.4. General procedure for the preparation of hydantoin (41–45)

To a stirring solution of the ketone (1.0 equiv) in 50% ethanol were added KCN (2.0 equiv) and ammonium carbonate (4.0 equiv). The reaction mixture was stirred at 60–65 °C for more than 24 h (using TLC to monitor reaction progress). When the reaction was completed, the reaction mixture was cooled to room temperature and extracted with CH₂Cl₂. The organic extracts were dried over MgSO₄, filtered, concentrated, and purified by silica gel column chromatography, eluting with EtOAc/hexane.

5.4.1. 2-Diethylamino-*N*-[4-(2,5-dioxo-4-phenyl-imidazolidin-4-yl)-phenyl]-acetamide (41)

Isolated as a white solid. mp 253–244 °C; ¹H NMR: δ 9.74–9.17 (s, 1H), 8.62–8.47 (s, 1H), 8.10–7.96 (s, 1H), 7.56–7.17 (m, 9H), 3.29–2.93 (s, 1H), 2.81–2.40 (m, 4H), 1.22–0.81 (t, J = 6 Hz, 6H); ¹³C NMR (CDCl₃): δ 175.47, 171.34, 164.91, 139.63, 138.02, 135.32, 129.17, 128.86, 128.22, 127.34, 120.11, 71.72, 58.37, 49.35, 12.86; HRMS (EI): calcd for C₂₁H₂₄N₄O₃ 380.4466; found, 380.4465.

5.4.2. 2-Diethylamino-*N*-[4-(2,5-dioxo-4-phenyl-imidazolidin-4-yl)-2,6-dimethyl-phenyl]-acetamide (42)

Isolated as a white solid, (61%); mp 164–167 °C; ¹H NMR: δ 10.46–9.82 (s, 1H), 9.56–8.76 (s, 2H), 7.70–6.47 (m, 7H), 3.42–3.04 (s, 2H), 2.90–2.52 (m, 4H), 2.53–2.16 (s, 6H), 1.29–0.92 (t, J = 7.5 Hz, 6H); ¹³C NMR (CDCl₃): δ 174.39, 173.13, 157.58, 141.43, 140.1, 128.55, 128.45, 128.04, 126.73, 126.63, 70.86, 57.44, 49.60, 19.35, 13.28; HRMS (EI): calcd for C₂₃H₂₈N₄O₃ 408.5003; found 408.5003.

5.4.3. 2-Diethylamino-*N*-[4-(4-hexyl-2,5-dioxo-imidazolidin-4-yl)-2,6-dimethyl-phenyl]-acetamide (43)

Isolated as a white solid (57%); mp 107–110 °C; ¹H NMR: δ 9.85–10.00 (b, 1H), 9.24–8.63 (s, 1H), 7.90–8.00 (b, 1H), 7.54–6.86 (s, 2H), 3.35–3.13 (s, 2H), 2.78–2.53 (m, 4H), 2.31–2.11 (s, 6H), 1.37–1.29 (m, 10H), 1.28–1.14 (t, J = 9.6 Hz), 0.94–0.67 (t, J = 6 Hz, 3H); ¹³C NMR: δ 176.48, 171.74, 158.08, 135.91, 133.99, 125.96, 125.42, 68.79, 57.67, 49.47, 31.95, 29.49, 23.09, 23.00, 19.20, 19.07, 14.62, 14.20; HRMS (EI): calcd for C₂₃H₃₆N₄O₃ 416.5636; found, 416.5633.

5.4.4. 2-Diethylamino-*N*-[4-(4-heptyl-2,5-dioxo-imidazolidin-4-yl)-2,6-dimethyl-phenyl]-acetamide (44)

Isolated as a light yellow solid (48%); mp 97–100 °C; ¹H NMR: δ 9.36–8.57 (s, 1H), 7.60–6.80 (s, 2H), 3.35–3.07 (s, 2H), 2.82–2.54 (m, 4H), 2.35–2.07 (s, 6H), 2.03–1.75 (m, 2H), 1.37–1.14 (m, 10H), 1.13–0.97 (t, J = 7.5 Hz, 6H), 0.95–0.67 (t, J = 6 Hz, 3H); ¹³C NMR: δ 176.44, 164.51, 157.93, 136.04, 136.01, 125.88, 125.77, 68.86, 57.72, 49.51, 32.23, 29.84, 29.48, 24.17, 23.06, 19.24, 14.54, 13.15; HRMS (EI): calcd for C₂₄H₃₈N₄O₃ 430.5907; found, 430.5905.

5.4.5. 2-Diethylamino-*N*-[2,6-dimethyl-4-(4-nonyl-2,5-dioxo-imidazolidin-4-yl)-phenyl]-acetamide (45)

Isolated as a white solid (78%); mp 95–98 °C; ¹H NMR: δ 9.23–8.79 (s, 1H), 8.11–7.86 (s, 1H), 7.81–7.47 (s, 1H), 7.31–6.98 (s,

2H), 3.33–3.02 (t, J = 9 Hz, 2H), 2.80–2.48 (m, 4H), 2.33–2.09 (s, 6H), 1.87–1.83 (m, 2H), 1.36–1.13 (m, 14H), 1.19–1.10 (t, J = 7.5 Hz, 6H), 0.92–0.68 (t, J = 6 Hz, 3H); ¹³C NMR: δ 176.58, 171.57, 164.61, 137.39, 135.83, 134.27, 125.66, 68.88, 60.78, 57.50, 53.90, 50.47, 49.30, 32.24, 31.97, 29.90, 29.74, 23.04, 19.10, 14.52, 12.76; HRMS (EI): calcd for C₂₆H₄₂N₄O₃ 458.6445; found, 458.6444.

5.5. Molecular modeling conformational analysis

The X-ray coordinates for phenytoin (DPH) were utilized in this study.¹⁴ The conformations of training set compounds **1–36** (Fig. 2) were determined as previously described.⁶ An additional 15 common local anesthetics were added to this model and modified from a representative X-ray structure. These modified structures were energy-minimized with the Tripos force field,¹⁵ without solvent, using default bond distances and angles and neglecting electrostatics. The minimization was completed by aggregating using the SYBYL/AGGREGATE module for only the X-ray structure atoms and allowing the modified portion to minimize. For internal consistency, we used only the *R*-configuration for all chiral compounds. The test set analogues **37–45** (Table 3) were modified in SYBYL using the X-ray conformation of lidocaine and representative low-energy conformations were obtained using the Tripos force field. To determine the low-energy conformations for **37–45**, we utilized GRIDSEARCH on rotatable bonds over 360° in 1° increments. The atomic charges for all analogues were calculated using AM1 (MOPAC).

5.6. Molecular alignment

Benzocaine, lidocaine, butacaine, cocaine, hexylcaine, piperocaine, parethoxycaine, and piperocaine utilized in the training set were fit to overlap the C1 and C4 carbons of the phenyl ring and the adjacent carbon or atom to C1. All hydantoin were fit as previously reported.⁶ Similarly, for analogues **41–45** in the test set, we aligned the C1 and C4 carbons of the phenyl ring and the adjacent nitrogen and the hydantoin ring was fit as previously described.⁶ The hydroxyamides **37–40** were aligned such that the OH group was superimposed with N1 and the carboxamide was aligned with C4 and N3. The *n*-alkyl groups at R₁ in analogues **37, 40, and 43–45** in the test set approximated a fully extended conformation following energy minimization, which was arbitrarily selected for this study.

5.7. CoMFA calculations

CoMFA, using default parameters except where noted, was calculated in the QSAR option of SYBYL 6.8 on a Silicon Graphics with an Octane II R12000 dual processor. The CoMFA grid spacing was 2.0 Å in the *x*, *y*, and *z* directions, and the grid region was automatically generated by the CoMFA routine to encompass all molecules with an extension of 4.0 Å in each direction. An sp³ carbon and a charge of +1.0 were used as probes to generate the interaction energies at each lattice point. The default value of 30 kcal/mol was used as the maximum electrostatic and steric energy cutoff.

5.8. Partial least squares (PLS) regression analysis

A single conformer for each compound was selected by the smallest cross-validated residual value. Single conformers of each training set compound were used in both the non-cross-validated model (Table 1) and the cross-validated model (Table 2). We also used the final non-cross-validated CoMFA model to predict the sodium channel binding activities for all low-energy conformations of the test set compounds **37–45** (Table 3).

Table 2
Cross-validated PLS analysis

Components	s	q ²
1	0.746	0.242
2	0.663	0.418
3	0.654	0.452
4	0.644	0.485
5	0.691	0.426
6	0.674	0.473

s, standard error for the estimate of logIC₅₀; q², correlation coefficient or press value = 1.0 - (Σ(Y predicted - Y actual)² ÷ (Y actual - Y mean)²). Optimum number of components is 4 with q² = 0.485.

Cross-validated (preliminary and final models) and non-cross-validated PLS analyses (final model) were performed within the SYBYL/QSAR routine. Cross-validation of the dependent column (pIC₅₀) and the CoMFA column was performed with 2.0 kcal/mol column filtering. Scaled by the CoMFA standard deviation, the final cross-validated analysis generated an optimum number of components equal to 4 and q² = 0.485 (Table 2). PLS analysis with non-cross-validation, performed with 4 components, gave a standard error of estimate of 0.245, a probability of R² = 0 (n₁ = 4, n₂ = 31) equal to 0.000, an F value (n₁ = 4, n₂ = 31) of 96, and a final q² = 0.926. The relative steric (0.624) and electrostatic (0.376) contributions to the final model were contoured as the standard deviation multiplied by the coefficient at 80% for favored steric (contoured in green) and favored positive electrostatic (contoured in blue) effects and at 20% for disfavored steric (contoured in yellow) and favored negative electrostatic (contoured in red) effects, as shown in Figure 5. On the basis of this analysis, the sodium channel binding activities for low-energy conformers of analogues 37–45, from the test set (Table 3), were predicted.

5.9. Chemistry

The synthesis of compounds 37–45 is shown in Scheme 1 and detailed in the experimental section. Briefly, the aminobenzophenones were generated by reaction of substituted anilines and acids in polyphosphoric acid (PPA). Subsequent reaction with diethylamine, NaHCO₃, and KI in MeOH generated the lidocaine-ketones which were carried on to final product amides and hydantoin.

Table 3
Predicted and actual sodium channel binding activities for novel grafted analogues forming the test set

Compound	R ₁	R ₂	Log P ^a	[³ H]-BTX Inhibition at 40 μM (%)	-pIC ₅₀		
					Obsd	Pred ^b	Res
37	<i>n</i> -Heptyl	Methyl	3.6	83 ± 1.53	-0.78	-0.85	-0.07
38	Phenyl	H	1.4	4 ± 4.56	nd	-1.82	
39	Phenyl	Methyl	2.4	16 ± 5.23	nd	-1.74	
40	<i>n</i> -Nonyl	Methyl	4.4	63 ± 1.01	nd	-0.51	
41	Phenyl	H	1.6	50 ± 0.92	-1.60	-1.65	-0.05
42	Phenyl	Methyl	2.5	49 ± 2.72	-1.60	-1.70	-0.10
43	<i>n</i> -Hexyl	Methyl	3.3	68 ± 4.26	nd	-1.09	
44	<i>n</i> -Heptyl	Methyl	3.7	71 ± 0.30	-1.13	-0.87	-0.26
45	<i>n</i> -Nonyl	Methyl	4.5	69 ± 0.89	nd	-0.59	

^a Calculated using the chemical properties tool of ChemDraw (CambridgeSoft, Inc.).

^b Data generated from the CoMFA non-cross-validated run (see QSAR methods).

5.10. Biological data

The structures and literature reference [³H]-BTX displacement data for compounds 1–20, the 15 local anesthetics (21–35), and phenytoin (36) that form the training set, are listed in Figure 2 and Table 1. Table 3 describes the structures and sodium channel binding activities of compounds 37–45, which form the test set.

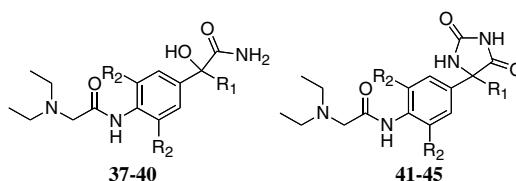
5.11. [³H]-BTX-B experiment

In the sodium channel evaluation, the IC₅₀, which represents the micromolar concentration of compound required to displace 50% of specifically bound [³H]-BTX) was determined using rat cerebral cortex synaptoneurosomes. To calculate the IC₅₀ value, the percent inhibition at 5–7 concentrations, which spanned the IC₅₀ value, was determined in triplicate and the IC₅₀ value was obtained by a Probit analysis of the concentration versus percent binding curve. Briefly, rat forebrain membranes were incubated with [³H]-Batrachotoxin (30–60 Ci/mmol). Reactions are carried out in 50 mM HEPES (pH 7.4) containing 130 mM choline chloride at 37 °C for 60 min. The reaction was terminated by rapid vacuum filtration of the reaction contents onto glass fiber filters. Radioactivity trapped onto the filters was determined and compared to control values in order to ascertain any interactions of the test compound with the sodium channel site 2 binding site. Aconitine [1 μM] was used as a positive control.

5.12. Cell culture and electrophysiology

Human embryonic cells (HEK) cells stably expressing human Na_v1.2 were grown in DMEM/F12 media (Invitrogen, Corp., CA, USA) supplemented with 10% fetal bovine serum, penicillin (100 U/ml), streptomycin (100 μg/ml) and G418 (500 μg/ml; Sigma, MO, USA). Cells were grown in a humidified atmosphere of 5% CO₂ and 95% air at 37 °C.

Sodium currents were recorded using the whole-cell configuration of the patch clamp recording technique with an Axopatch 200B amplifier (Axon Instruments, Foster City, CA). All voltage protocols were applied using pCLAMP 8 software (Axon, USA) and a Digidata 1322A (Axon, USA). Currents were amplified and low pass filtered (2 kHz) and sampled at 33 kHz. Borosilicate glass pipettes were pulled using a Brown–Flaming puller (model P87, Sutter



Instruments Co., Novato, CA) and heat polished to produce electrode resistances of 0.5–1.5 M Ω when filled with the following electrode solution (in mM); CsCl 130, MgCl₂ 1, MgATP 5, BAPTA 10, HEPES 5 (pH adjusted to 7.4 with CsOH). Cells were plated on glass coverslips and superfused with solution containing the following composition; (in mM) NaCl 130, KCl 4, CaCl₂ 1, MgCl₂ 5, HEPES 5, and glucose 5 (pH adjusted to 7.4 with NaOH).

Compounds were prepared as 100 mM stock solutions in Dimethyl sulfoxide (DMSO) and diluted to desired concentration in perfusion solution. The maximum DMSO concentration used was 0.3% and had no effect on current amplitude. All experiments were performed at room temperature (20–22 °C). After establishing whole-cell, a minimum series resistance compensation of 75% was applied.

Acknowledgments

We thank the NIH R01 NIH CA105435-0, Jeffress Trust Fund and the Paul Mellon Fund for financial support. We appreciate the technical support provided on the [³H]-BTX-B studies from Novascreen, Inc., (Tammy Ranson and Dr. Charles Bauer).

References and notes

1. Goldin, A. L. *Annu. Rev. Physiol.* **2001**, *63*, 871.
2. McNeal, E. T.; Lewandowski, G. A.; Daly, J. W.; Creveling, C. R. *J. Med. Chem.* **1985**, *28*, 381.
3. Worley, P. F.; Baraban, J. M. *Proc. Nat. Acad. Sci. U.S.A.* **1987**, *84*, 3051.
4. Brouillette, W. J.; Jestkov, V. P.; Brown, M. L.; Akhtar, M. S.; DeLorey, T. M.; Brown, G. B. *J. Med. Chem.* **1994**, *37*, 3289.
5. Brown, M. L.; Brown, G. B.; Brouillette, W. J. *J. Med. Chem.* **1997**, *40*, 602.
6. Brown, M. L.; Zha, C. C.; Van Dyke, C. C.; Brown, G. B.; Brouillette, W. J. *J. Med. Chem.* **1999**, *42*, 1537.
7. Vamecq, J.; Bac, P.; Herrenknecht, C.; Maurois, P.; Delcourt, P.; Stables, J. P. *J. Med. Chem.* **2000**, *43*, 1311.
8. Wang, S. Y.; Barile, M.; Wang, G. K. *Mol. Pharmacol.* **2001**, *59*, 1100.
9. Yarov-Yarovoy, V.; McPhee, J. C.; Idsvoog, D.; Pate, C.; Scheuer, T.; Catterall, W. A. *J. Biol. Chem.* **2002**, *277*, 35393.
10. Yarov-Yarovoy, V.; Brown, J.; Sharp, E. M.; Clare, J. J.; Scheuer, T.; Catterall, W. A. *J. Biol. Chem.* **2001**, *276*, 20.
11. Ragsdale, D. S.; McPhee, J. C.; Scheuer, T.; Catterall, W. A. *Proc. Nat. Acad. Sci. U.S.A.* **1996**, *93*, 9270.
12. Kuo, C. C. *Mol. Pharmacol.* **1998**, *54*, 712.
13. Kaczorowski, G. J.; McManus, O. B.; Priest, B. T.; Garcia, M. L. *J. Gen. Physiol.* **2008**, *131*, 399.
14. Camerman, A.; Camerman, N. *Acta Crystallogr.* **1971**, *B27*, 2205.
15. Clark, M. D.; Cramer, R. D., III; Opdenbosch, N. V. *J. Comput. Chem.* **1989**, *10*, 982.